RSC Advances

PAPER

View Article Online
View Journal | View Issue

Cite this: *RSC Adv.*, 2020, **10**, 20960

Study on the properties of perovskite materials under light and different temperatures and electric fields based on DFT

Xin-Feng Diao, *[abc] Yan-lin Tang,*[a] De-Yong Xiong,[b] Ping-Rui Wang,[b] Li-ke Gao,[a] Tian-yu Tang,[a] Xiao-Nan Wei,[a] Hai-Rong Zhang,[b] Xu-Pu wu[b] and Shen-Tong Ji[b]

The photoelectric conversion efficiency of perovskite solar cells has improved rapidly, but their stability is poor, which is an important factor that restricts their commercial production. This paper studies the physical and chemical stability of perovskite solar cells based on first principles. It is well known that methylamido lead iodide compounds and methylamino lead iodide compounds are easily degraded into $NH_2CH{=}NH_2I$, CH_3NH_3I and PbI_2. First, the chemical stability of the above two perovskite-type solar cell materials is discussed by calculating the binding energy. Then, their phonon scattering lines, state density and thermodynamic properties are calculated and analyzed, and the work functions of different types of crystals along different planes such as [1 0 0], [0 1 0 0], [0 0 1] and [1 1 1] are calculated. The results show that the work function of the methylamine iodized lead compound is greater than that of the methylamidine iodized lead compound, which means that the electrons of the methylamidine iodized lead compound escape more easily and the carrier transfer efficiency is higher under the same conditions. Finally, the effects of different temperatures, different electric fields and light on the two kinds of crystal materials are analyzed. This provides theoretical guidance for us to improve the stability of perovskite materials experimentally.

Received 31st March 2020
Accepted 26th May 2020

DOI: 10.1039/d0ra02841j

rsc.li/rsc-advances

1 Introduction

In recent years, the increasing demand for photovoltaic products has brought opportunities for new photovoltaic technologies. So far, the development of solar cells has gone through three generations: silicon-based cells, multi-component composite thin film cells, organic thin film solar cells and dye-sensitized solar cells. Perovskite solar cells (PSCs), as the third generation of solar cells, have attracted wide attention due to the continuous improvement of power conversion efficiency (PCE), low material cost and simple manufacturing process.[1–6] PSC, which first appeared in 2009 with an efficiency of 3.8%, has achieved a laboratory-scale photoelectric conversion efficiency of 25.2%.[7–10] Perovskite solar cells have a broad development prospect, but the main reason perovskite solar cells cannot be used on a large scale is the battery stability. At present, perovskite-type solar cells can only work for several months under active conditions, while conventional silicon cells can work for more than 25 years. How to improve the stability of perovskite batteries and make them as good as commercial polysilicon solar cells is the most important problem in the field of perovskite solar cells. The instability of organic–inorganic hybrid perovskite, such as the volatilization of organic cations in $(MAPbI_3)\cdot CH_3NH_3PbI_3$ and $(FAPbI_3)\cdot NH_2CH{=}NH_2PbI_3$ under thermal stress, has become a major limiting factor for its long-term practical application. Ze Wang *etc.*[11] studied the effects of ambient temperature and humidity on the chemical stability of perovskites, and found that the degradation reaction $CH_3NH_3PbI_3 \rightarrow CH_3NH_3I + PbI_2$ and $CH_3NH_3I \rightarrow CH_3NH_2 + HI$ would occur when $MAPbI_3$ was exposed to light illumination and different temperatures. Nick Aristidou and his colleagues[12] investigated the moisture stability mechanisms of perovskite solar cell materials in a mixture of water and oxygen. In fact, it is not known whether the iodine and hydrogen atoms in the perovskite materials are more readily dissociated to form PbI_2 and HI ions. In this paper, the formation energy in the degradation reaction is calculated based on the first principle, which can help us analyze which dissociation reaction is easier to carry out. That's something you can't do experimentally. At the same time, the phonon dispersion spectrum, density of states and thermodynamic properties of the crystals are calculated and analyzed. The work functions of different types of crystals along different planes [1 0 0] [0 1 0][0 0 1] [1 1 1] are also calculated. Finally, the effects of different temperature, different electric field and light on the two kinds of crystal materials are analyzed.

[a]School of Physics, Guizhou University, Guiyang, 550025, China. E-mail: tylgzu@163.com; diaoxinfeng77@126.com

[b]School of Physics and Electronic Sciences, Guizhou Normal College, Guiyang 550018, China

[c]School of Big Data and Information Engineering, Guizhou University, Guiyang 550025, China

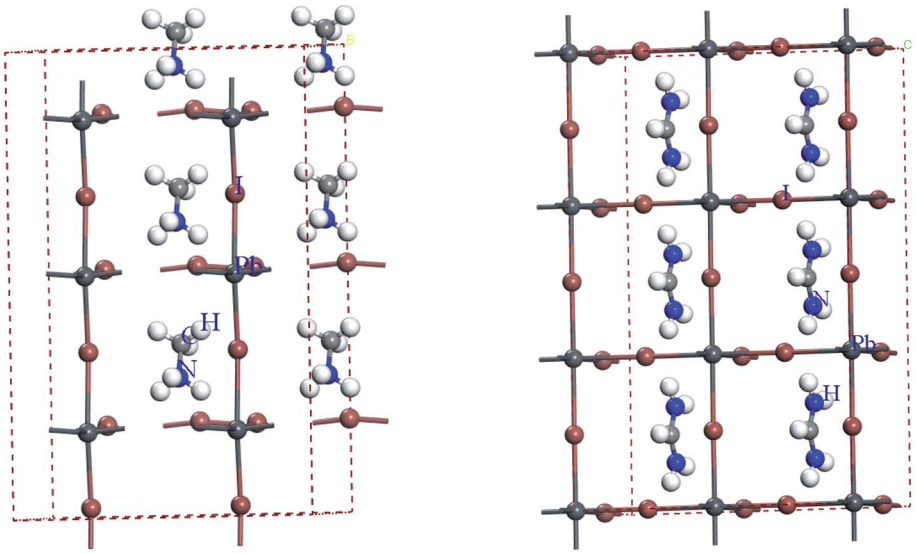

$CH_3NH_3PbI_3$ (a) $NH_2CH{=}NH_2PbI_3$ (b)

Fig. 1 Structure diagram of two crystals.

This provides theoretical guidance for us to improve the stability of perovskite materials experimentally.

For convenient observation of crystal structure, we build the supercells of two crystals with $2 \times 3 \times 1$ mesh which was shown as Fig. 1, and the lattice parameters are as following: (a) $a = 12.58$ Å, $b = 18.69$ Å, $c = 6.37$ Å, $\alpha = 90.00°$, $\beta = 88.74°$, $\gamma = 89.98°$, (b) $a = 12.82$ Å, $b = 19.01$ Å, $c = 6.27$ Å, $\alpha = \beta = \gamma = 90°$. Space group crystal system of two crystals are triclinic.

2 Computational methods

In this paper, two perovskite crystal materials $NH_2CH{=}NH_2PbI_3$ and $CH_3NH_3PbI_3$ were calculated based on DFT method, and the simulation package (CASTEP and $Dmol^3$) was used to complete the calculation. The part from 3.1 to 3.4 in this paper is calculated by the CASTEP module.[13–15] The exchange–correlation effects were still treated by Perdew–Burke–Ernzerh (PBE) of function in the generalized gradient approximation (GGA).[16,17] The cut-off energy of plane wave basis set is 340 eV, and the SCF (self-consistent field) tolerance of the total energy change of each atom is set as 1×10^{-5} eV per atom. The maximum force of each atom is less than 0.01 eV $Å^{-1}$ and the optimization is less than 0.0005 Å. The existence of tightly bound core electrons is represented by supersoft pseudopotential.[18,19] The integral of Brillouin region is replaced by the discrete summation of a set of special K points using Monkhorst–pack scheme. And in the part 3.5, the study on the properties of applying electric field to crystals are calculated by $Dmol^3$ package. And the details of the calculations were as follows: the exchange–correlation effects were treated by Generalized Gradient Approximation (GGA) version of Perdew–Wang-1991(PW91),[20] and the basis set was 3.5 double numerical plus d-functions basis (DND), the qualities were selected as "fine".

3 Results and discussion

3.1. Thermal stability studies

With the improvement of the understanding of the instability of component materials under the conditions of humidity, heat, light and oxygen, more researches have been carried out on the long-term stability of perovskite materials.[21–28] Perovskite materials degrade rapidly when exposed to humid environment.[29–34] Our previous work[35] has explored the structural stability of perovskite crystal and its adsorption properties for water molecules. Many papers[36–39] reported that the perovskite materials $CH_3NH_3PbI_3$ and $NH_2CH{=}NH_2PbI_3$ will decompose into CH_3NH_2, $NH_2CH{=}NH$, PbI_2 and HI at above 150 °C. The decomposition of perovskite is the reverse reaction of perovskite formation, and the instability caused by humidity and heat generally exists in organic–inorganic hybrid perovskite. The current mixed perovskite is facing another challenge: they are unstable to light.[40–44] The possible mechanism of decomposition on exposure to light is as follows

$$CH_3NH_3PbI_3 \xrightarrow{h\nu} CH_3NH_3I + PbI_2 \quad (1)$$

$$NH_2CHaNH_2PbI_3 \xrightarrow{h\nu} NH_2CHaNH_2I + PbI_2 \quad (2)$$

In the superlattices of $MAPbI_3$ and $FAPbI_3$, there is one lead (Pb) atom, three iodine(I) atoms and one group. However, the dissociation energies of I atoms at different positions are not equal. We can use formation energy to express its stability. If the absolute value of crystal formation energy is small, it indicates that its stability is poor. The formula of formation energy can be written as follows:

$$\Delta E = E_{CH_3NH_3PbI_3} - E_{CH_3NH_3I} - E_{PbI_2} \quad (3)$$

Table 1 Formation energy of $CH_3NH_3PbI_3$

	$CH_3NH_3PbI_3$		CH_3NH_3I	PbI_2	
Degradation pathway 1	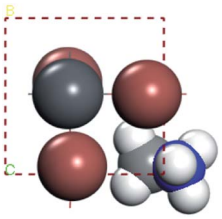	$\xrightarrow{hv}$	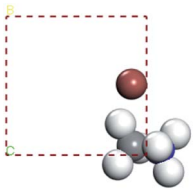	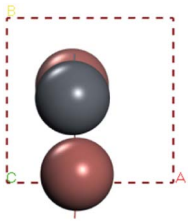	ΔE
	−3125.36 eV		−837.04 eV	−2287.04 eV	−1.28 eV
Degradation pathway 2	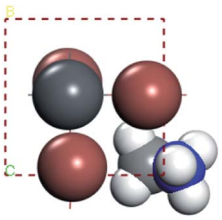	$\xrightarrow{hv}$	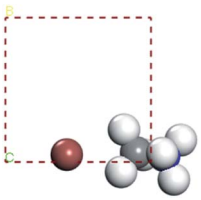	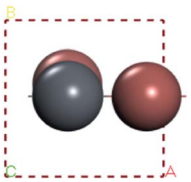	ΔE
	−3125.36 eV		−836.89 eV	−2287.03 eV	−1.44 eV
Degradation pathway 3	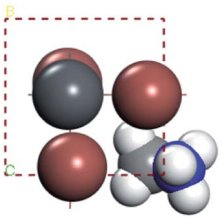	$\xrightarrow{hv}$	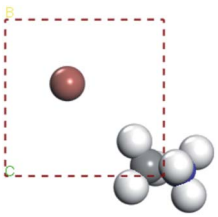	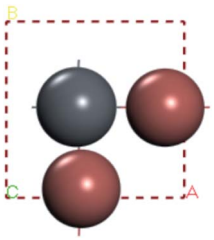	ΔE
	−3125.36 eV		−836.93 eV	−2287.03 eV	−1.40 eV

where $E_{CH_3NH_3PbI_3}$, $E_{CH_3NH_3I}$, E_{PbI_2} are the optimized energy of the crystal. The total energy of reaction for degradation pathways in a number of different ambient environments are calculated by DFT methods and shown in Table 1.

It can be seen from Table 1 that $CH_3NH_3PbI_3$ absorbing light and heat is decomposed into CH_3NH_2I and PbI_2. The energy required to dissociate ions at different positions of the crystal is not equal, and its magnitude is −1.28 eV, −1.44 eV and −1.40 eV, respectively. The results show that the first form of degradation is more likely to occur. For $NH_2CH{=}NH_2PbI_3$ crystal, the formation energy can be expressed as:

$$\Delta E = E_{CH_3NH_3I} - E_{CH_3NH_2} - E_{HI} \quad (4)$$

We know that $NH_2CH{=}NH_2PbI_3$ absorbs energy to decomposed into $NH_2CH{=}NH_2I$ and PbI_2. The dissociation of I and Pb atoms at different locations requires different energies to form PbI_2. The greater the absolute value of the energy required for dissociation, the more difficult the reaction. Table 2 shows that these three reaction formation energies are −1.28 eV, −0.95 eV and −1.53 eV, respectively. The result shows that the second form of degradation is easier to occur, while the third form of degradation is the most difficult.

The possible mechanism of further decomposition on exposure to the environments of light illumination, different temperatures which is as follows[11]:

$$CH_3NH_3I \xrightarrow{hv} CH_3NH_2 + HI \text{ or } CH_3NH_3I \xrightarrow{hv} CH_2NH_3 + HI \quad (5)$$

$$NH_2CHaNH_2I \xrightarrow{hv} NH_2CHaNH + HI \text{ or } NH_2CHaNH_2I \xrightarrow{hv} NH_2CaNH_2 + HI \quad (6)$$

We further analyzed the dissociation energies required for ion separation at different sites to help us explore which chemical reactions are more likely to occur. The different hydrogen (H) and iodine (I) atoms in the crystal are labeled as follows. Consider the combination of hydrogen (H) ions and iodine (I) atoms in different positions to form HI as a product. The difficulty of this reaction is determined by calculating the formation energies of the reactants and products.

$$\Delta E = E_{CH_3NH_3I} - E_{CH_3NH_2} - E_{HI} \text{ or } \Delta E = E_{CH_3NH_3I} - E_{CH_2NH_3} - E_{HI} \quad (7)$$

$$\Delta E = E_{NH_2CH=NH_2I} - E_{NH_2CH=NH} - E_{HI} \text{ or } \Delta E = E_{NH_2CH=NH_2I} - E_{NH_2C=NH_2} - E_{HI} \quad (8)$$

Table 2 Formation energy of $NH_2CH{=}NH_2PbI_3$

	$NH_2CH{=}NH_2PbI_3$		$NH_2CH{=}NH_2I$	PbI_2	
Degradation pathway 1	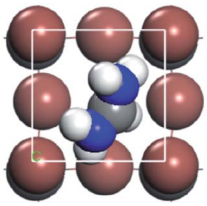	$\xrightarrow{hv}$	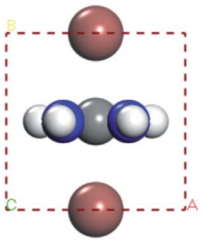	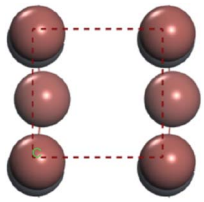	ΔE
	−3380.1 eV		−1091.68 eV	−2287.14 eV	−1.28 eV
Degradation pathway 2	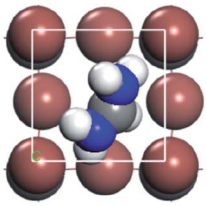	$\xrightarrow{hv}$	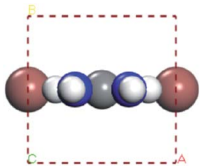	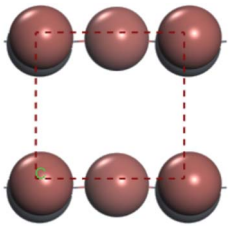	ΔE
	−3380.1 eV		−1092.10 eV	−2287.05 eV	−0.95 eV
Degradation pathway 3	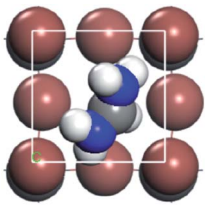	$\xrightarrow{hv}$	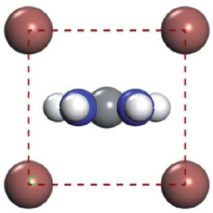	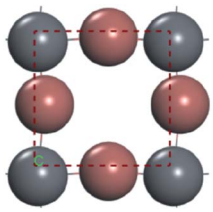	ΔE
	−3380.1 eV		−1091.52 eV	−2287.05 eV	−1.53 eV

where $E_{CH_3NH_3I}$, $E_{NH_2CH=NH_2I}$ are the optimized energy of reactants, and $E_{NH_2CH=NH}$, $E_{CH_3NH_2}$, E_{HI}, are the optimized energy of products.

In this part, we can discuss the possibility of its further degradation reaction by calculating its formation energy, and the results shown in Tables 3 and 4. For convenience, we have

Table 3 Formation energy of CH_3NH_3I

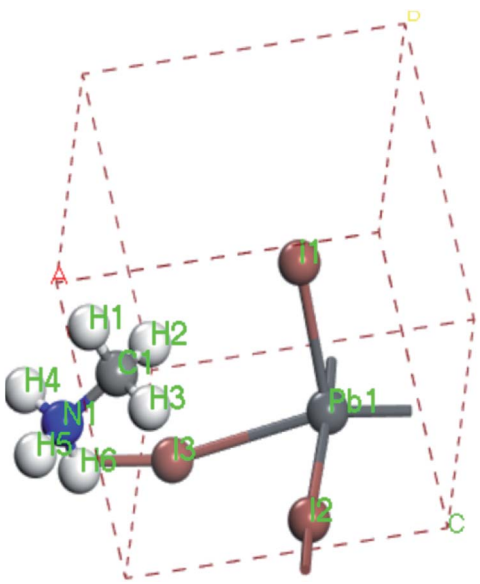

	$CH_2NH_3 + H^1I^1$ (a)	$CH_2NH_3 + H^1I^2$ (b)	$CH_2NH_3 + H^1I^3$ (c)
ΔE (eV)	−6.01	−6.36	−5.73
	$CH_2NH_3 + H^2I^1$ (d)	$CH_2NH_3 + H^2I^2$ (e)	$CH_2NH_3 + H^2I^3$ (f)
ΔE (eV)	−7.64	−6.33	−4.72
	$CH_2NH_3 + H^3I^1$ (g)	$CH_3NH_2 + H^3I^2$ (h)	$CH_3NH_2 + H^3I^3$ (i)
ΔE (eV)	−6.32	−6.20	−6.37
	$CH_3NH_2 + H^4I^1$ (j)	$CH_3NH_2 + H^4I^2$ (k)	$CH_3NH_2 + H^4I^3$ (l)
ΔE (eV)	−6.13	−6.24	−6.39
	$CH_3NH_2 + H^5I^1$ (m)	$CH_3NH_2 + H^5I^2$ (n)	$CH_3NH_2 + H^5I^3$ (o)
ΔE (eV)	−6.35	−6.33	−6.46
	$CH_3NH_2 + H^6I^1$ (p)	$CH_3NH_2 + H^6I^2$ (q)	$CH_3NH_2 + H^6I^3$ (r)
ΔE (eV)	−5.51	−6.47	−7.60

Table 4 Formation energy of $NH_2CH{=}NH_2I$

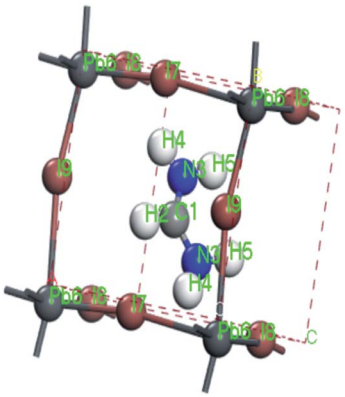

	$NHCH = NH_2 + H^4I^7$ (A)	$NHCH = NH_2 + H^4I^8$ (B)	$NHCH = NH_2 + H^4I^9$ (C)
ΔE (eV)	−12.48	−12.95	−12.21
	$NHCH = NH_2 + H^5I^7$ (D)	$NHCH = NH_2 + H^5I^8$ (E)	$NHCH = NH_2 + H^5I^9$ (F)
ΔE (eV)	−12.44	−13.02	−11.52
	$NH_2C{=}NH_2 + H^2I^7$ (G)	$NH_2C{=}NH_2 + H^2I^8$ (H)	$NH_2C{=}NH_2 + H^2I^9$ (I)
ΔE (eV)	−7.05	−7.13	−6.97

numbered each atom in the crystal, as shown in left figure in the table. The superscript number of the element indicates the position number of the atom in the crystal, such as H^1I^1.

The results show that the combination of H^4, H^5, and H^6 with iodide (I) ions is unstable, and it is easier to decompose into H^+ and I^- ions. From the left figure of Table 3, it can be seen that the hydrogen atom at positions 4, 5 and 6 is outside the supercell. The HI formed by iodine is unstable. This kind of iodine amine compound is easier to dissociate and has poor stability. The font color in Table 3 is blue, indicating that the product HI is unstable. They are easy to generate as H_2 and I_2

It can be seen from Fig. 2 this reaction of $CH_2NH_3 + H^2I^3$ is easier to carry out, and I_2 and H_2 gas will continue to be generated. And then the easier degraded reactions were (c) $CH_2NH_3 + H^1I^3$ and (p) $CH_3NH_2 + H^6I^1$.

Compared with the energy required for various degradation reactions in Table 4, the energy required for further dissociation of amidine iodide is in the order of (I) < (G) < (H) < (F) < (C) < (D) < (A) < (B) < (E). The reactions of (G), (H) and (I) are more likely to occur. This result is even more obvious in Fig. 3. And the degradation reaction of eqn (6) is more difficult than that of eqn (5).

For convenience, we define eqn (1) and (2) as first-order degradation reactions and eqn (5) and (6) as second-order degradation reactions. It can be seen that the energy required for the primary degradation reaction is 1.56 eV, while the energy required for the secondary degradation reaction is greater than 6.24 eV, indicating that the secondary degradation reaction is more difficult than the primary degradation reaction.

3.2. Research on thermodynamic properties

In order to further study the stability of these two kinds of crystals, we optimized their phonon dispersion spectrum and distribution curve of phonon density of state, as shown in Fig. 4. First of all, the structure is optimized by using the CASTEP package, then the phonon dispersion spectrum, density of states and thermodynamic properties of two kinds of crystals are calculated and obtained.

In Fig. 4 (a) and (b), zero point energy of $CH_3NH_3PbI_3$ is 2.09 eV, which is slightly larger than that of $NH_2CH{=}NH_2PbI_3$ (1.902 eV). The free energy of the two crystals decreases with the increase of temperature. Their enthalpy increases with the

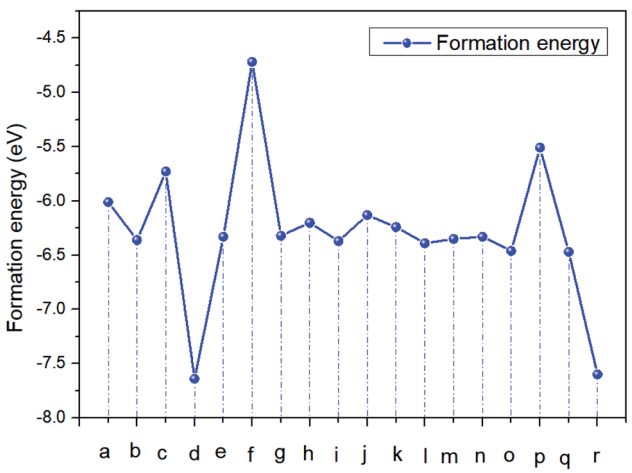

Fig. 2 Formation energy curve of CH_3NH_3I.

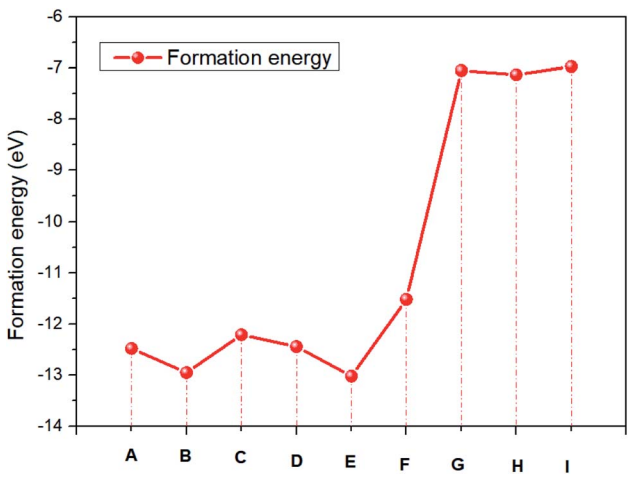

Fig. 3 The formation energy of $NH_2CH{=}NH_2I$.

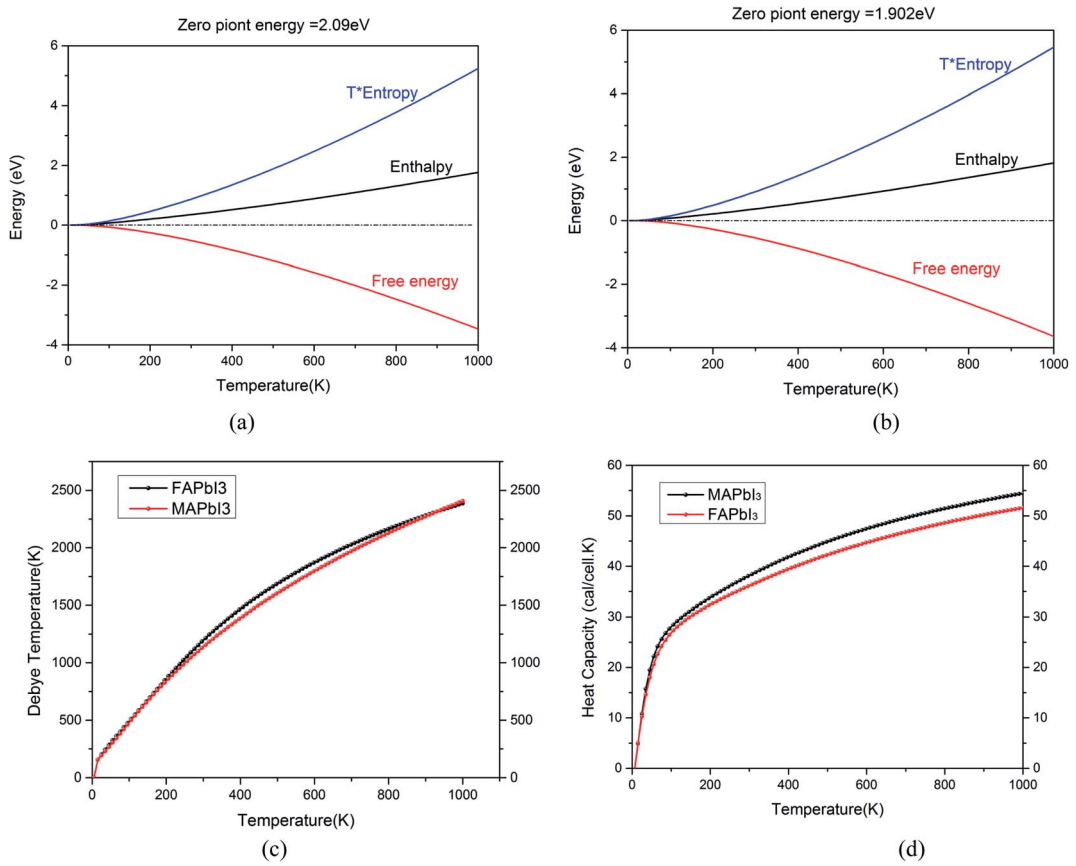

Fig. 4 (a) Thermodynamic properties of $CH_3NH_3PbI_3$, (b) thermodynamic properties of $NH_2CH{=}NH_2PbI_3$, (c) Debye temperature of two crystals, (d) heat capacity of two crystals.

increase of temperature. Fig. 4(c) shows that the Debye temperature corresponds to the highest frequency of lattice vibration. It is actually a characteristic quantity of the strongest bond between crystals. Which can reflect the size of the bonding force between atoms. The Debye temperature of different materials is different, the melting point is high, that is, the stronger the atomic bond of the material is, the higher the Debye temperature is. It can be seen from Fig. 4(d) that the change trend of the bond energy between atoms of the two crystals is basically the same with the increase of temperature. The binding capacity of $NH_2CH{=}NH_2PbI_3$ is slightly higher than $CH_3NH_3PbI_3$. The heat capacity of $NH_2CH{=}NH_2PbI_3$ is lower than that of $CH_3NH_3PbI_3$.

3.3. Phonon spectrum of crystals

It can be inferred from Fig. 5 that $CH_3NH_3PbI_3$ and $NH_2CH{=}NH_2PbI_3$ are unstable because they have imaginary frequencies in the phonon spectrum, which is consistent with their small formation energy (see Tables 1 and 2). Also it tells us that phonon spectrum band gap of $CH_3NH_3PbI_3$ is similar as that of $NH_2CH{=}NH_2PbI_3$. However, the frequency of $MAPbI_3$ is between 45 and 85 THz, and the frequency of $FAPbI_3$ is between 52 and 92 THz. We know that with the decrease of the moment of inertia of the oscillator, the natural frequency of the oscillator will increase and the position frequency of the local resonance band gap will also increase. The position frequency of the local resonance band gap caused by the rotating oscillator is close to the fixed frequency of the oscillator. However, different from the linear displacement oscillator, with the decrease of the dimensionless mass, the band width shows an increasing trend. And rotational inertia of $FAPbI_3$ is smaller than that of $MAPbI_3$.

3.4. Calculation of work function

In our calculations, the metal slab is placed in the center of a cell and a 20 Å vacuum is introduced along the z direction. In the following, our approach to calculate the electrochemical potential and the total energy will be given in detail. In order to calculate the electrochemical potential (U) of a system, the following equations can be used according to the definition of absolute electrochemical potential. The work function reflects the minimum energy required for electrons to move from the interior of a solid to the surface of the object, $CH_3NH_3PbI_3 \xrightarrow{hv} CH_3NH_3I + PbI_2$, where E_{VAC} is the energy of a static electron in a vacuum and EF is Fermi level. Since the work function W depends on the crystal structure and crystal orientation, the crystal structure of the bulk material should be optimized before the two-dimensional array is constructed. So we build two kinds of crystals along different surface [0 0 1][0 1 0][1 0 0][1 1 1]. And a vacuum layer with a thickness of 20 Å, fix the surface atoms, and optimize the crystal structure, then

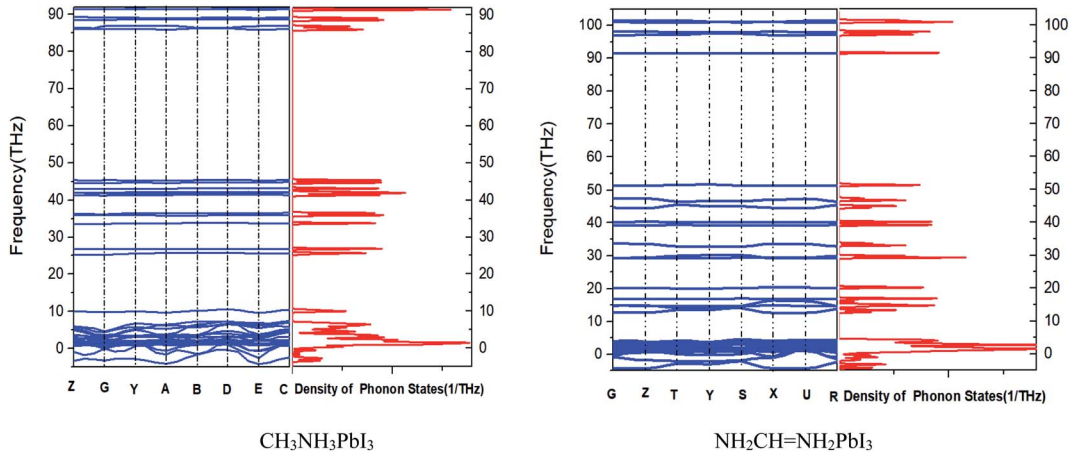

$CH_3NH_3PbI_3$ $NH_2CH{=}NH_2PbI_3$

Fig. 5 Phonon dispersion and density of states of two kinds of crystals.

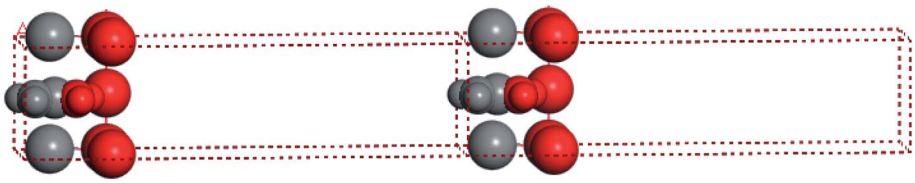

Fig. 6 $FAPbI_3$ cleave surface [1 0 0].

calculate the corresponding work function, as shown in the following Fig. 6:

For comparison purposes, I constructed a vacuum layer (20 Å) for $FAPbI_3$ and $MAPbI_3$ crystal. In the calculation results of $FAPbI_3$, the electrostatic energy values of the vacuum top electron and the vacuum bottom electron appear on the plane [1 0 0] and [1 1 1] respectively. Its operating function is between 5.811–3.799 eV and 6.238–5.552 eV. In $MAPbI_3$, the work function has no obvious fluctuation, and the surface work function is 5.054 eV, 4.96 eV, 5.946 eV, 5.194 eV at surface [0 0 1], [0 1 0],

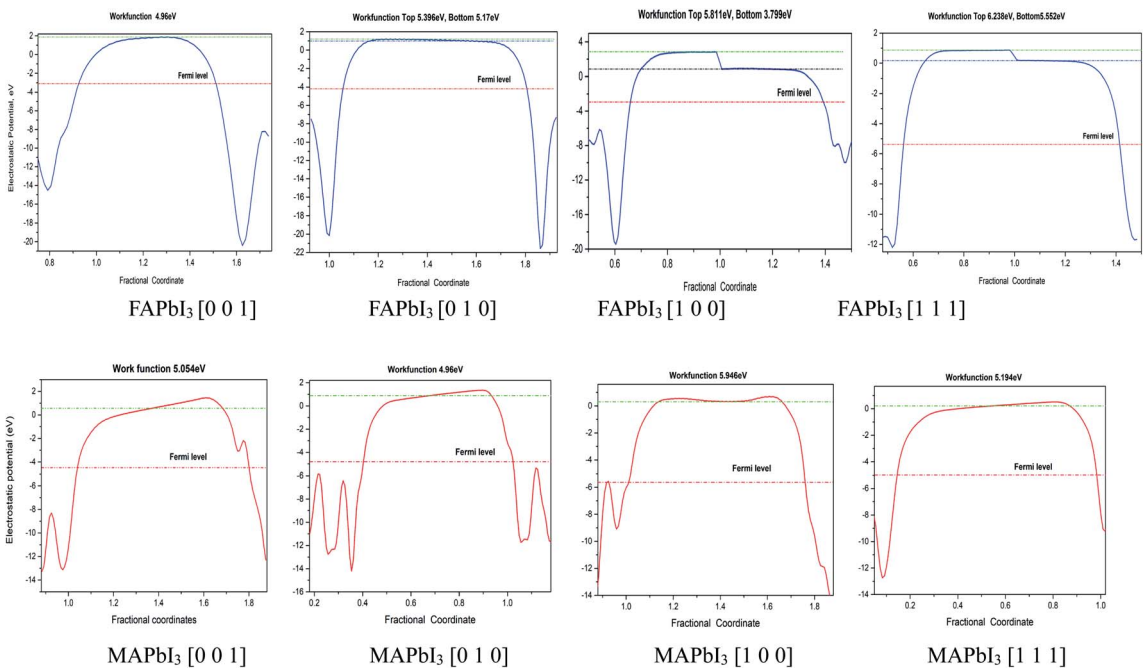

Fig. 7 Thermodynamic properties of two kinds of crystals.

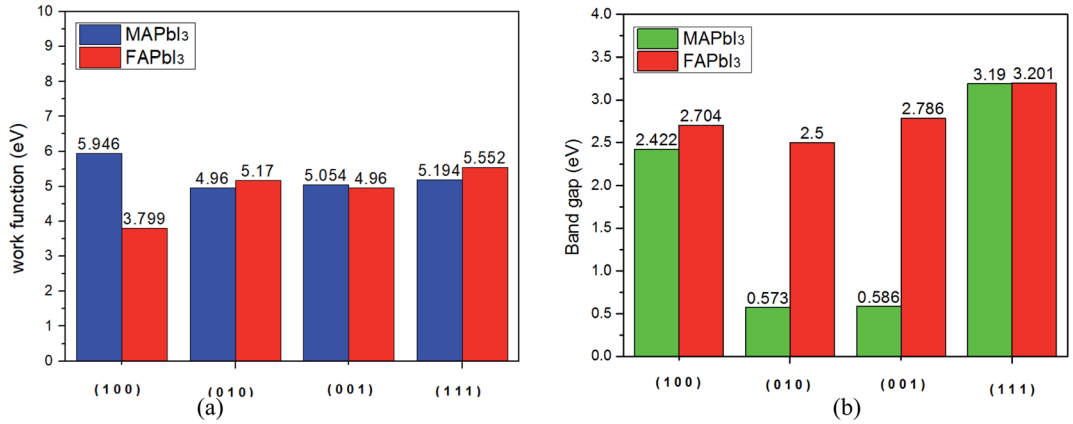

Fig. 8 (a) Work function and (b) band gap of two kinds of crystals.

[1 0 0], [1 1 1], respectively. Also we can find that the work function of $MAPbI_3$ is greater than that of $FAPbI_3$ for [1 0 0] plane, the work functions in other planes for $FAPbI_3$ and $MAPbI_3$ crystal are similar, as shown in the Fig. 7.

From Fig. 8(a), we find that the work function of $FAPbI_3$ has a minimum value (3.799 eV) along the [1 0 0] plane, while the work function of $MAPbI_3$ is the minimum value in the [0 1 0] plane. We further explored the changes of band gap on different cutting planes, which were [1 0 0], [0 1 0], [0 0 1], and [1 1 1], and calculated the corresponding band gap using CASTEP module. As can be seen from Fig. 8(b), the band gap of $MAPbI_3$ varies greatly along different cleavage planes, while the band gap of $FAPbI_3$ varies little.

3.5. Perovskite crystal stability at different temperatures

As solar cells, they are exposed to the sun all year round and their temperature varies greatly. It is necessary to analyze the influence of temperature on perovskite materials. We can now focus on the analysis of different environments (250 K, 273 K, 300 K 350 K, 373 K, 400 K, 450 K) to calculate their free energy and kinetic energy to analyze the change of crystal stability at different temperatures. The result shows as Fig. 9(a) and (b).

For macroscopic systems such as crystals, the principle follows the lowest free energy $F = U-TS$, where U is the potential energy and TS is the kinetic energy. Fig. 10 tells us that $MAPbI_3$ obtain the minimum kinetic energy at a temperature of 273 K (0 °C) and the maximum value at 373 K (100 °C). $FAPbI_3$ also achieved a maximum at 373 K (100 °C). And $FAPbI_3$ suddenly increased to −3379.80 eV at 273 K (0 °C), which means that the stability of this crystal decreased at 0 °C. The free energy for $MAPbI_3$ does not change much at different temperatures.

3.6. Apply an electric field in different directions

Perovskite solar cells always work at a certain voltage, so we discuss the effect of electric field on the crystal stability in different directions. Because the CASETP package of material Studio software cannot analyze the application electric field during calculation, but the $Dmol^3$ package can apply an electric field to the bulk crystal. In this part, we use the $Dmol^3$ package for calculation, and the parameter setting is described in part 2. After applying the electric field 0.005 a.u or 0.01 a.u. in the x, y and z directions, the corresponding free energy, bond energy, exchange energy, kinetic energy of the system molecule, Fermi energy level, conduction band and valence state are obtained (1 a.u. $\approx 5.14 \times 10^{11}$ V m^{-1}).

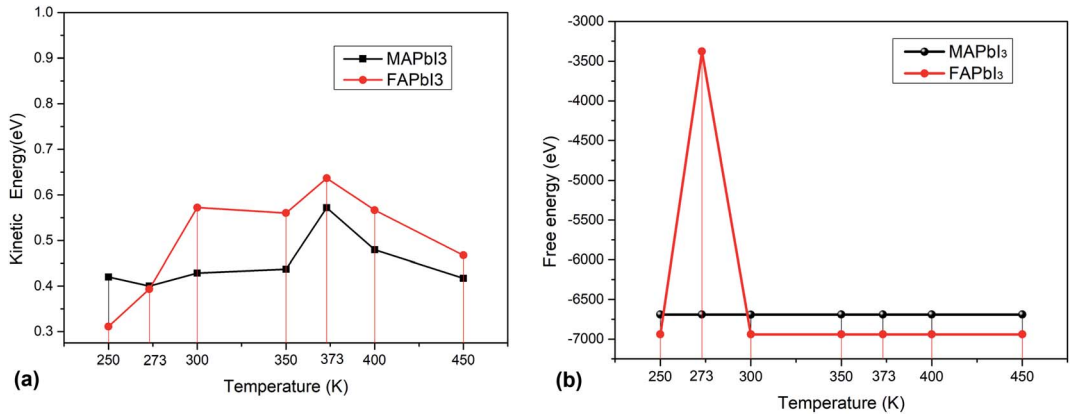

Fig. 9 (a) Kinetic energy and (b) free energy of crystals at different temperatures.

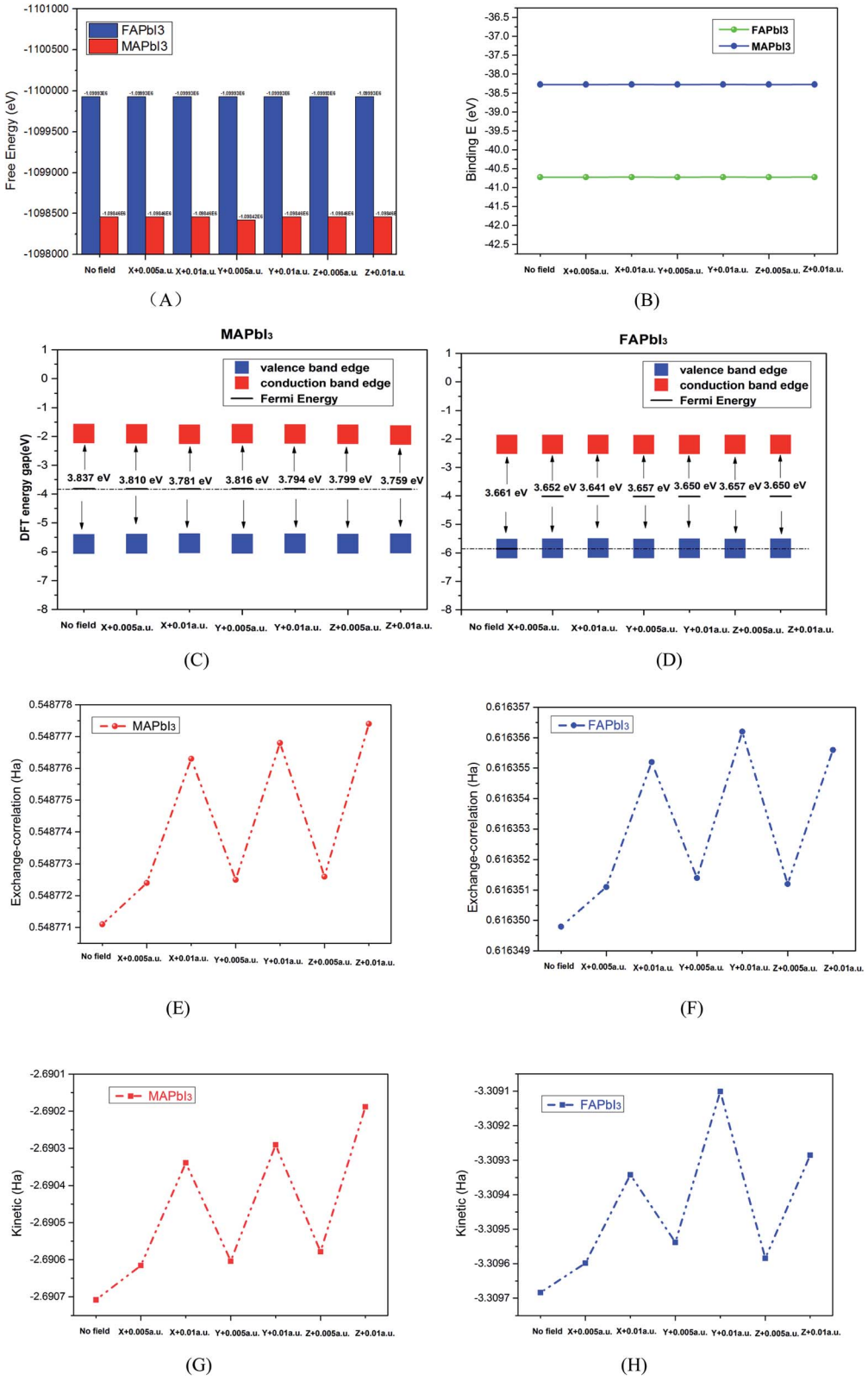

Fig. 10 (A)–(H) are thermodynamic properties of two kinds of crystals.

The calculation results are shown in Fig. 10(A–H). It can be seen from Fig. 10(A) that the system free energy of crystal $FAPbI_3$ is higher than that of $MAPbI_3$. Fig. 10(B) shows that the bond energy of $FAPbI_3$ is lower than that of $MAPbI_3$. Because the bonding energy is lower, its stability is relatively poor, and the naturally the free energy is high, which is consistent with the

theory of solid physics. Fig. 10(E–H) shows that the free energy and bond energy of the electric field have little change after the application of the electric field, which means that the electric field has little influence on its stability. However, after the electric field is applied, its Fermi level position increases slightly, as shown in Fig. 10(C) and (D). The Fermi energy level increases with the increase of voltage. When the electric field is applied along the *z*-axis, the change is more obvious. From the point of view of molecular kinetic energy and exchange energy of the system, the energy increases significantly after the application of electric field, and increases with the increase of voltage.

4 Conclusion

In this paper, the stability of two important organic–inorganic perovskite solar cell materials, $FAPbI_3$ and $MAPbI_3$, under different light, temperature and electric field were studied in detail. Firstly, the chemical degradation reactions of the two organic–inorganic perovskite crystals material

$$CH_3NH_3PbI_3 \xrightarrow{hv} CH_3NH_3I + PbI_2 \text{ and } NH_2CHaNH_2PbI_3 \xrightarrow{hv} NH_2CHaNH_2I + PbI_2$$

were studied under heat condition. Moreover, the photoactive layer of $CH_3NH_3PbI_3$ and $NH_2CH{=}NH_2PbI_3$ can be rapidly decomposed into a Al_2O_3 mesoporous structures under light and drying conditions, generating products such as CH_3NH_2, $NH_2CH{=}NH_2$, HI and I_2. Since iodine (I) atoms in different parts of the crystal need different energies to react with hydrogen, which reaction form is more likely to occur can be determined according to the energy required for the reaction. By calculating the formation energy, it is found that $CH_3NH_3PbI_3$ is more likely to undergo the first type of degradation reaction, while $NH_2CH{=}NH_2PbI_3$ is more likely to undergo the second type of degradation reaction. The above results cannot be specifically determined by experiments. Furthermore, 18 possible CH_3NH_3I degradation reactions and 9 possible $NH_2CH{=}NH_2I$ degradation schemes were analyzed. The calculation results show that the hydrogen atoms H^4, H^5, and H^6 are not stable in combination with iodine ions, and are easier decompose into H^+ and I^- ions. It can be seen from the figure that the reactions of (G), (H) and (I) are more likely to occur when the hydrogen atoms at positions 4, 5 and 6 are outside the supercell unit.

Then, the phonon dispersion spectrum, thermodynamic properties, and work functions of the two crystals are discussed. The phonon dispersion curve shows that the moment of inertia of $FAPbI_3$ is smaller than that of $MAPbI_3$. The $FAPbI_3$ system has the maximum free energy and kinetic energy at 373 K (100 °C), but the free energy of $MAPbI_3$ does not change much at different temperatures. The free energy of $FAPbI_3$ suddenly increases to −3379.80 eV at 273 K (0 °C), which means that it has the lowest temperature dependence at 0 °C. The work function of $MAPbI_3$ is greater than that of $FAPbI_3$ for [1 0 0] plane, which means that the electrons of $FAPbI_3$ are easier to escape and its carrier transfer efficiency is higher with the same conditions. In other planes, the work functions of the two crystals are similar.

Finally, the stability of the two kinds of crystals under different temperature and electric field is discussed. The free energy of crystal $FAPbI_3$ is higher than that of $MAPbI_3$. When the electric field is applied, the free energy and bond energy of the two crystals do not change significantly, which means that the electric field has little influence on their stability. However, the molecular kinetic energy and exchange energy of the two crystalline materials increase obviously and increase with the increase of the voltage. This provides theoretical guidance for us to improve the stability of perovskite materials experimentally.

Conflicts of interest

There are no conflicts to declare.

Acknowledgements

This work is supported by the National Natural Science Foundation of China Program (Grant No. 11164004), Guizhou Provincial Photonic Science and Technology Innovation team (Qianke Joint talents team [2015]4017), the Industrial Research Project of Guizhou Province (GY[2012]3060), the Growth Foundation for Young Scientists of Guizhou Provincial Department of Education (Grant no. QJH KY [2018]265), Special Laboratory Fund of Guizhou Education Department of Education (GY[2014] 217), First class discipline education science construction project of Guizhou Education University [2019YLXK C05]

References

1 A. Kojima, K. Teshima, Y. Shirai and T. Miyasaka, Organometal Halide Perovskites as Visible-Light Sensitizers for Photovoltaic Cells, *J. Am. Chem. Soc.*, 2009, **131**(17), 6050–6051, DOI: 10.1021/ja809598r.

2 H. S. Kim, C. R. Lee, J. H. Im, K. B. Lee, T. Moehl, A. Marchioro, *et al.*, Lead Iodide Perovskite Sensitized All-Solid-State Submicron Thin Film Mesoscopic Solar Cell with Efficiency Exceeding 9%, *Sci. Rep.*, 2012, **2**(1), 591, DOI: 10.1038/srep00591.

3 S. Alessandro, M. Igor and M. Joachim, Short-range ion dynamics in methylammonium lead iodide by multinuclear solid state NMR and 127 I NQR, *Phys. Chem. Chem. Phys.*, 2018, **20**(30), 20043–20055, DOI: 10.1039/C8CP01535J.

4 M. M. Lee, J. Teuscher, T. Miyasaka, T. N. Murakami and H. J. Snaith, Efficient Hybrid Solar Cells Based on Meso-Superstructured Organometal Halide Perovskites, *Science*, 2012, **338**(6107), 643–647.

5 J. F. Yang, X. M. Wen, H. Z. Xia, R. Sheng, Q. S. Ma, J. C. Jincheol Kim, P. Tapping, T. Harada, T. W. Kee, F. Z. Huang, Y. B. Cheng, M. Green, H. B. Anita, S. J. Huang, S. Shrestha, P. Robert and C. Gavin, A coustic-optical phonon up-conversion and hot-phonon bottleneck in lead-halide perovskites, *Nat. Commun.*, 2017, **8**, 14120, DOI: 10.1038/ncomms14120.

6 V. Roiati, S. Colella, G. Lerario, L. De Marco, A. Rizzo, A. Listorti and G. Gigli, Energy Environ. Investigating

charge dynamics in halide perovskite-sensitized mesostructured solar cells, *Energy Environ. Sci.*, 2014, **7**, 1889–1894, DOI: 10.1039/C3EE43991G.

7 P. Basera, M. Kumar, S. Saini and S. Bhattacharya, Reducing lead toxicity in the methylammonium lead halide $MAPbI_3$:Why Sn substitution should be preferred to Pb vacancy for optimum solar cell efficiency, *Phys. Rev. B*, 2020, **101**, 054108, DOI: 10.1103/PhysRevB.101.054108.

8 N. G. Park, M. Grätzel, T. Miyasaka, K. Zhu and K. Emery, Towards stable and commercially available perovskite solar cells, *Nat. Energy*, 2016, **1**(11), 16152, DOI: 10.1038/nenergy.2016.152.

9 W. S. Yang, B. Park, E. H. Jung and N. J. Jeon, Iodide management in formamidinium-lead-halide-based perovskite layers for efficient solar cells, *Science*, 2017, **356**, 1376–1379, DOI: 10.1126/science.aan2301.

10 National Renewable Energy Laboratory, *Best Research-Cell Efficiencies*, 2019, www.nrel.gov/pv/assets/pdfs/pv-efficiency-chart.20190103.pdf.

11 Z. Wang, Z. J. Shi, T. T. Li, Y. H. Chen and W. Huang, Stability of Perovskite Solar Cells: A Prospective on the Substitution of the ACation and XAnion, *Angew. Chem.*, 2016, **129**(5), 1210–1233, DOI: 10.1002/anie.201603694.

12 N. Aristidou, C. Eames, M. S. Islam and S. A. Haque, Insights into the increased degradation rate of $CH_3NH_3PbI_3$ solar cells in combined water and O_2 environments, *J. Mater. Chem. A*, 2017, **5**, 25469–25475, DOI: 10.1039/c7ta06841g.

13 D. Vanderbilt, Soft self-consistent pseudopotentials in a generalized eigenvalue formalism, *Phys. Rev. B: Condens. Matter Mater. Phys.*, 1990, **41**, 7892–7895, DOI: 10.1103/PhysRevB.41.7892.

14 G. Giacomo, I. F. Jun and S. S. Hiroshi, Small Photocarrier Effective Masses Featuring Ambipolar Transport in Methylammonium Lead Iodide Perovskite: A Density Functional Analysis, *J. Phys. Chem. Lett.*, 2013, **4**, 4213–4216, DOI: 10.1021/jz4023865.

15 K. Kaasbjerg, K. S. Thygesen and K. W. Jacobsen, Phonon-limited mobility in n-type single-layer MoS_2 from first principles, *Phys. Rev. B: Condens. Matter Mater. Phys.*, 2012, **85**, 115317, DOI: 10.1103/physrevb.85.115317.

16 M. D. Segall, P. J. D. Lindan, M. J. Probert, C. J. Pickard, P. J. Hasnip, S. J. Clark and M. C. Payne, First-principles simulation: ideas, illustrations and the CASTEP code, *J. Phys.: Condens. Matter*, 2002, **14**, 2717–2744, DOI: 10.1088/0953-8984/14/11/301.

17 S. J. Clark, M. D. Segall, C. J. Pickard, P. J. Hasnip, M. I. J. Probert, K. Refson and M. C. Payne, First principles methods using CASTEP, *Z. Kristallogr.*, 2005, **220**, 567–570, DOI: 10.1524/zkri.220.5.567.65075.

18 J. P. Perdew, K. Burke and M. Ernzerhof, Generalized Gradient Approximation Made Simple, *Phys. Rev. Lett.*, 1996, **77**, 3865–3868, DOI: 10.1103/PhysRevLett.77.3865.

19 H. J. Monkhorst and J. D. Pack, Special points for Brillouin-zone integrations, *Phys. Rev. B*, 1976, **13**, 5188–5192, DOI: 10.1103/PhysRevB.13.5188.

20 X. F. Diao, Y. L. Tang, Q. Xie, D. L. Chen, S. X. Li and G. F. Liu, Study on the Property of Electron-Transport Layer in the Doped Formamidinium Lead Iodide Perovskite Based on DFT, *ACS Omega*, 2019, **4**, 20024–20035, DOI: 10.1021/acsomega.9b03015.

21 P. Docampo and T. Bein, A Long-Term View on Perovskite Optoelectronics, *Acc. Chem. Res.*, 2016, **49**, 339–346, DOI: 10.1021/acs.accounts.5b00465.

22 Y. Rong, L. Liu, A. Mei, X. Li and H. Han, Beyond Efficiency: the Challenge of Stability in Mesoscopic Perovskite Solar Cells, *Adv. Energy Mater.*, 2015, **5**, 1501066, DOI: 10.1002/aenm. 201501066.

23 T. Leijtens, G. E. Eperon, N. K. Noel, S. N. Habisreutinger, A. Petrozza and H. J. Snaith, Stability of Metal Halide Perovskite Solar Cells, *Adv. Energy Mater.*, 2015, **5**, 1500963, DOI: 10.1002/aenm.201500963.

24 T. A. Berhe, W. Su, C. Chen, C. Pan, J. Cheng, H. Chen, M. Tsai, L. Chen, A. A. Dubale and B. Hwang, Organometal halide perovskite solar cells: degradation and stability, *Energy Environ. Sci.*, 2016, **9**, 323–356, DOI: 10.1039/C5EE02733K.

25 M. Ye, X. Hong, F. Zhang and X. Liu, Recent advancements in perovskite solar cells: flexibility, stability and large scale, *J. Mater. Chem. A*, 2016, **4**, 6755–6771, DOI: 10.1039/C5TA09661H.

26 N. H. Tiep, Z. L. Ku and H. J. Fan, Recent advances in improving the stability of perovskite solar cells, *Adv. Energy Mater.*, 2016, **6**, 1501420, DOI: 10.1002/aenm. 201501420.

27 F. Brivio, J. M. Frost, J. M. Skelton, A. J. Jackson, O. J. Weber, M. T. Weller, A. R. Goni, A. M. A. Leguy, P. R. F. Barnes and A. Walsh, Lattice dynamics and vibrational spectra of the orthorhombic, tetragonal, and cubic phases of methylammonium lead iodide, *Phys. Rev. B: Condens. Matter Mater. Phys.*, 2015, **92**, 144308, DOI: 10.1103/PhysRevB.92.144308.

28 B. Li, Y. Li, C. Zheng, D. Gao and W. Huang, Advancements in the stability of perovskite solar cells: degradation mechanisms and improvement approaches, *RSC Adv.*, 2016, **6**, 38079–38091, DOI: .

29 J. H. Noh, S. H. Im, J. H. Heo, T. N. Mandal and S. II Seok, Chemical Management for Colorful, Efficient, and Stable Inorganic–Organic Hybrid Nanostructured Solar Cells, *Nano Lett.*, 2013, **13**, 1764–1769, DOI: 10.1021/nl400349b.

30 G. Niu, W. Li, F. Meng, L. Wang, H. Dong and Y. Qiu, Study on the stability of $CH_3NH_3PbI_3$ films and the effect of post-modification by aluminum oxide in all-solid-state hybrid solar cells, *J. Mater. Chem. A*, 2014, **2**, 705–710, DOI: 10.1039/C3TA13606J.

31 C. Clegg and I. G. Hill, Systematic study on the impact of water on the performance and stability of perovskite solar cells, *RSC Adv.*, 2016, **6**, 52448–52458, DOI: 10.1039/C6RA11379F.

32 Y. Zhang, P. P. Heng, H. S. Su, J. F. Li, J. Guo, P. Ning, W. P. Wu, T. G. Ren, L. Wang and J. L. Zhang, Star-Shaped Molecules as Dopant-Free Hole Transporting Materials for Efficient Perovskite Solar Cells: Multiscale Simulation Chem, *Rec*, 2019, **19**, 938–946, DOI: 10.1002/tcr.201800150.

33 W. Y. Zhang, L. Wang, L. M. Mao, J. M. Jiang, H. H. Ren, P. P. Heng, H. A. Ågren and J. L. Zhang, Computational

Protocol for Precise Prediction of Dye-Sensitized Solar Cell Performance, *J. Phys. Chem. C*, 2020, **124**, 3980–31, DOI: 10.1021/acs.jpcc.9b10869.

34 Y. Zhang, J. Guo, H. S. Su, J. F. Li, W. P. Wu and L. Wang, A rational design of hole-transport small molecules based on fluorene with different modified groups for organic lead-halide perovskite solar cells, *Dyes Pigm.*, 2018, **154**, 275–281, DOI: 10.1016/j.dyepig.2018.03.019.

35 X. F. Diao, Y. L. Tang, T. Y. Tang, Q. Xie, K. Xiang and G. F. Liu, Study on the stability of organic–inorganic perovskite solar cell materials based on first principle, *Mol. Phys.*, 2019, e1665200, DOI: 10.1080/00268976.2019.1665200.

36 B. Conings, J. Drijkoningen, N. Gauquelin, A. Babayigit, J. D'Haen, L. D'Olieslaeger, A. Ethirajan, J. Verbeeck, J. Manca, E. Mosconi, F. De Angelis and H. Boyen, Intrinsic Thermal Instability of Methylammonium Lead Trihalide Perovskite, *Adv. Energy Mater.*, 2015, **5**, 1500477, DOI: 10.1002/aenm.201500477.

37 Y. Dkhissi, S. Meyer, D. Chen, H. C. Weerasinghe, L. Spiccia, Y. Cheng and R. A. Caruso, Stability Comparison of Perovskite Solar Cells Based on Zinc Oxide and Titania on Polymer Substrates, *ChemSusChem*, 2016, **9**, 687–695, DOI: 10.1002/cssc.201501659.

38 J. H. Heo, S. H. Im, J. H. Noh, T. N. Mandal, C. Lim, J. A. Chang, Y. H. Lee, H. Kim, A. Sarkar, M. K. Nazeeruddin, M. Graetzel and S. I. Seok, Efficient inorganic-organic hybrid heterojunction solar cells containing perovskite compound and polymeric hole conductors, *Nat. Photonics*, 2013, **7**, 487–492, DOI: 10.1038/nphoton.2013.80.

39 G. Divitini, S. Cacovich, F. Matteocci, L. Cin, A. Di Carlo and C. Ducati, In situ observation of heat-induced degradation of perovskite solar cells, *Nat. Energy*, 2016, **1**, 15012, DOI: 10.1038/NENERGY. 2015.12.

40 D. Bryant, N. Aristidou, S. Pont, I. Sanchez-Molina, T. Chotchunangatchaval, S. Wheeler, J. R. Durrant and S. A. Haque, Light and oxygen induced degradation limits the operational stability of methylammonium lead triiodide perovskite solar cells, *Energy Environ. Sci.*, 2016, **9**, 1655–1660, DOI: 10.1039/C6EE00409A.

41 H. Yuan, E. Debroye, K. Janssen, H. Naiki, C. Steuwe, G. Lu, M. Moris, E. Orgiu, H. Uji-i, F. De Schryver, P. Samori, J. Hofkens and M. Roeffaers, Degradation of Methylammonium Lead Iodide Perovskite Structures through Light and Electron Beam Driven Ion Migration, *J. Phys. Chem. Lett.*, 2016, **7**, 561–566, DOI: 10.1021/acs.jpclett.5b02828.

42 T. Leijtens, G. E. Eperon, S. Pathak, A. Abate, M. M. Lee and H. J. Snaith, Overcoming ultraviolet light instability of sensitized TiO_2 with meso-superstructured organometal tri-halide perovskite solar cells, *Nat. Commun.*, 2013, **4**, 2885, DOI: 10.1038/ncomms3885.

43 S. Ito, S. Tanaka, K. Manabe and H. Nishino, Effects of Surface Blocking Layer of Sb_2S_3 on Nanocrystalline TiO_2 for $CH_3NH_3PbI_3$ Perovskite Solar Cells, *J. Phys. Chem. C*, 2014, **118**, 16995–17000, DOI: 10.1021/jp500449z.

44 D. Wei, T. Wang, J. Ji, M. Li, P. Cui, Y. Li, G. Li, J. M. Mbengue and D. Song, Photo-induced degradation of lead halide perovskite solar cells caused by the hole transport layer/metal electrode interface, *J. Mater. Chem. A*, 2016, **4**, 1991–1998, DOI: 10.1039/C5TA08622A.